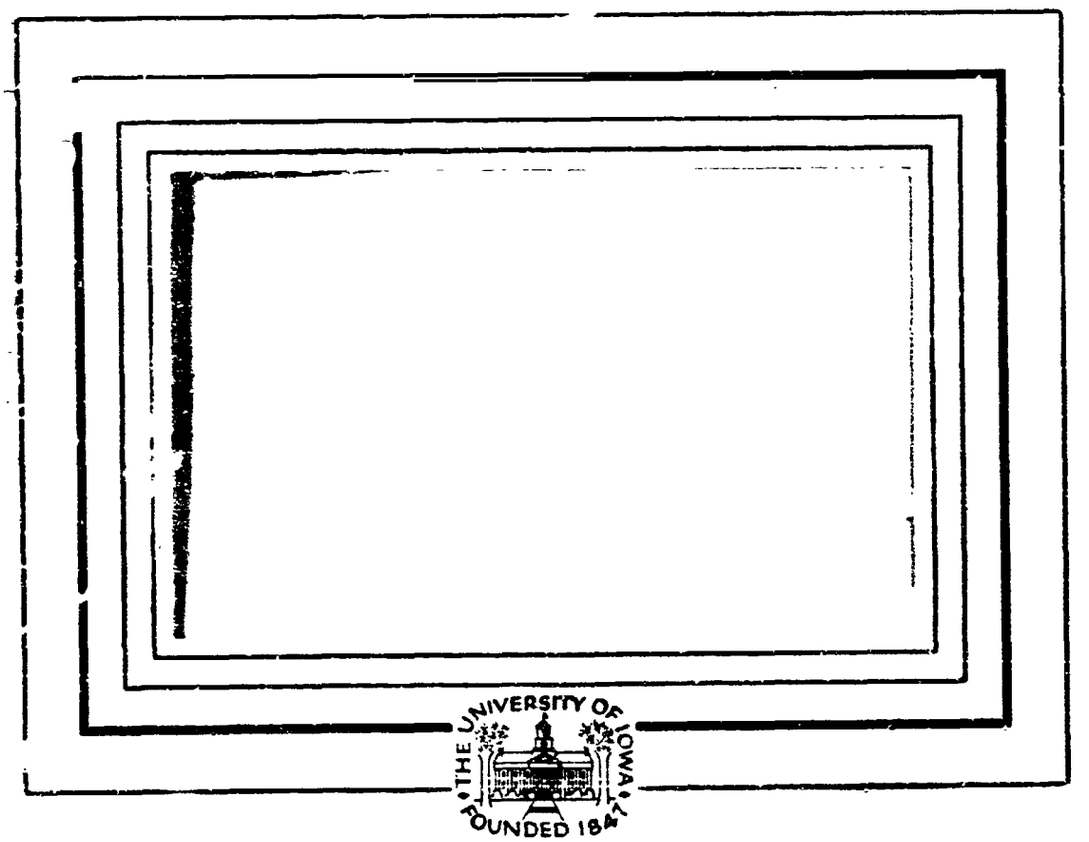

Department of Physics and Astronomy

THE UNIVERSITY OF IOWA

Iowa City, Iowa 52242

U. of Iowa 73-37

Thermal and Suprathermal Plasma Densities in the Outer Magnetosphere

by

D. A. Gurnett and L. A. Frank

October 1973

Department of Physics and Astronomy
The University of Iowa
Iowa City, Iowa 52242

This work was supported in part by the National Aeronautics and Space Administration under Contract NAS5-11074 and NAS5-11039 and Grant NGL-16-001-043 and by the Office of Naval Research under Grant N00014-68-A-0196-0009.

UNCLASSIFIED

Security Classification

DOCUMENT CONTROL DATA - R&D

(Security classification of title, body of abstract and indexing annotation must be entered when the overall report is classified)

1 ORIGINATING ACTIVITY (Corporate author)	2a REPORT SECURITY CLASSIFICATION
Department of Physics and Astronomy University of Iowa	UNCLASSIFIED 2b GROUP

3 REPORT TITLE

"Thermal and Suprathermal Plasma Densities in the Outer Magnetosphere"

4 DESCRIPTIVE NOTE (Type of report and inclusive dates)

Progress, October 1973

5 AUTHOR(S) (Last name, first name, initial)

Gurnett, Donald A., and Louis A. Frank

6 REPORT DATE	7a TOTAL NO OF PAGES	7b NO OF REFS
October 1973	28	16

8a CONTRACT OR GRANT NO	9a ORIGINATOR'S REPORT NUMBER(S)
N00014-68-A-0196-0009 b PROJECT NO c d	U. of Iowa 73-37 9b OTHER REPORT NO(S) (Any other numbers that may be assigned this report)

10 AVAILABILITY/LIMITATION NOTICES

Approved for public release; distribution is unlimited.

11 SUPPLEMENTARY NOTES	12 SPONSORING MILITARY ACTIVITY
	Office of Naval Research

13 ABSTRACT

[See following page]

DD FORM 1 JAN 64 1473

UNCLASSIFIED

Security Classification

14 KEY WORDS	LINK A		LINK B		LINK C	
	ROLE	WT	ROLE	WT	ROLE	WT
Thermal						
Suprathermal						
Outer Magnetosphere						

INSTRUCTIONS

1. ORIGINATING ACTIVITY: Enter the name and address of the contractor, subcontractor, grantee, Department of Defense activity or other organization *(corporate author)* issuing the report.

2a. REPORT SECURITY CLASSIFICATION: Enter the overall security classification of the report. Indicate whether "Restricted Data" is included. Marking is to be in accordance with appropriate security regulations.

2b. GROUP: Automatic downgrading is specified in DoD Directive 5200.10 and Armed Forces Industrial Manual. Enter the group number. Also, when applicable, show that optional markings have been used for Group 3 and Group 4 as authorized.

3. REPORT TITLE: Enter the complete report title in all capital letters. Titles in all cases should be unclassified. If a meaningful title cannot be selected without classification, show title classification in all capitals in parenthesis immediately following the title.

4. DESCRIPTIVE NOTES: If appropriate, enter the type of report, e.g., interim, progress, summary, annual, or final. Give the inclusive dates when a specific reporting period is covered.

5. AUTHOR(S): Enter the name(s) of author(s) as shown on or in the report. Enter last name, first name, middle initial. If military, show rank and branch of service. The name of the principal author is an absolute minimum requirement.

6. REPORT DATE: Enter the date of the report as day, month, year; or month, year. If more than one date appears on the report, use date of publication.

7a. TOTAL NUMBER OF PAGES: The total page count should follow normal pagination procedures, i.e., enter the number of pages containing information.

7b. NUMBER OF REFERENCES: Enter the total number of references cited in the report.

8a. CONTRACT OR GRANT NUMBER: If appropriate, enter the applicable number of the contract or grant under which the report was written.

8b, 8c, & 8d. PROJECT NUMBER: Enter the appropriate military department identification, such as project number, subproject number, system numbers, task number, etc.

9a. ORIGINATOR'S REPORT NUMBER(S): Enter the official report number by which the document will be identified and controlled by the originating activity. This number must be unique to this report.

9b. OTHER REPORT NUMBER(S): If the report has been assigned any other report numbers *(either by the originator or by the sponsor)*, also enter this number(s).

10. AVAILABILITY/LIMITATION NOTICES: Enter any limitations on further dissemination of the report, other than those imposed by security classification, using standard statements such as:

(1) "Qualified requesters may obtain copies of this report from DDC."

(2) "Foreign announcement and dissemination of this report by DDC is not authorized."

(3) "U. S. Government agencies may obtain copies of this report directly from DDC. Other qualified DDC users shall request through _____."

(4) "U. S. military agencies may obtain copies of this report directly from DDC. Other qualified users shall request through _____."

(5) "All distribution of this report is controlled. Qualified DDC users shall request through _____."

If the report has been furnished to the Office of Technical Services, Department of Commerce, for sale to the public, indicate this fact and enter the price, if known.

11. SUPPLEMENTARY NOTES: Use for additional explanatory notes.

12. SPONSORING MILITARY ACTIVITY: Enter the name of the departmental project office or laboratory sponsoring *(paying for)* the research and development. Include address.

13. ABSTRACT: Enter an abstract giving a brief and factual summary of the document indicative of the report, even though it may also appear elsewhere in the body of the technical report. If additional space is required, a continuation sheet shall be attached.

It is highly desirable that the abstract of classified reports be unclassified. Each paragraph of the abstract shall end with an indication of the military security classification of the information in the paragraph, represented as *(TS)*, *(S)*, *(C)*, or *(U)*

There is no limitation on the length of the abstract. However, the suggested length is from 150 to 225 words.

14. KEY WORDS: Key words are technically meaningful terms or short phrases that characterize a report and may be used as index entries for cataloging the report. Key words must be selected so that no security classification is required. Identifiers, such as equipment model designation, trade name, military project code name, geographic location, may be used as key words but will be followed by an indication of technical context. The assignment of links, rules, and weights is optional.

ABSTRACT

Using the low-frequency cutoff of electromagnetic noise trapped in the magnetosphere at frequencies above the local plasma frequency it is now possible to make very accurate, $\pm$ 1%, electron density measurements in the low density region between the magnetopause and plasmapause. This technique for measuring the total plasma density has been used, together with measurements of the suprathermal proton intensities with the LEPEDEA instrumentation on the IMP-6 spacecraft, to determine the thermal proton densities in the region between the plasmapause and magnetopause. Although the thermal protons usually account for a significant fraction, ~ 50%, of the total proton density in this region, in some cases, particularly at the larger radial distances the density of the thermal protons sometimes drops to a very small fraction, < 5%, of the total density and nearly all of the plasma consists of suprathermal particles.

Usually the high-energy tail of the thermal proton distribution is sufficiently intense to be detected at low energies within the LEPEDEA energy range. When the high-energy tail of the thermal distribution can be detected, it is possible to determine the temperature of the thermal protons. The temperature in a typical case is found to be 80,000°K. This high temperature for the thermal protons which are presumably of ionospheric origin agrees with earlier OGO-5 measurements reported by Serbu and Maier.

I. INTRODUCTION

The ratio of the cold thermal plasma density to the hot suprathermal plasma density plays a crucial role in the stability of magnetospheric plasmas [Kennel and Petschek, 1966; Cornwall et al., 1970; Brice and Lucas, 1971]. Qualitative comparisons of the thermal and suprathermal plasma densities have been made by Russell and Thorne [1970], using observations reported by Frank [1967a] and Taylor et al., [1968]. These data show that the hot ring-current protons penetrate deep into the cold ionospheric plasma inside the plasmapause during a geomagnetic storm. The region of overlap between the cold ionospheric plasma and the hot ring-current plasma is unstable for ion-cyclotron waves which resonate with the ring-current protons [Cornwall et al., 1970]. Similarly, the penetration of suprathermal electrons into the plasmasphere is believed to cause plasmaspheric hiss, via the resonant interaction of these electrons with whistler-mode waves [Thorne et al., 1973]. In both cases the presence of the cold plasma contributes significantly to the instability by lowering the energy at which resonance occurs, thereby increasing the number of particles which are in resonance with the wave.

Although there have been numerous independent measurements of both the cold plasma [Taylor et al., 1968; Serbu and Maier, 1970; Chappell et al., 1971] and the hot suprathermal plasma [Frank, 1967b; Vasyliunas, 1968; DeForest and McIlwain, 1971] there have been no

simultaneous measurements of both the thermal and suprathermal plasma densities in the low density region between the plasmapause and magnetopause with sufficient accuracy to be useful for quantitative investigations of the plasma instabilities which occur in this region. The purpose of this paper is to present a series of total electron density measurements using data from the University of Iowa plasma wave experiment on IMP-6, and simultaneous measurements of the suprathermal, 52 eV $\leq$ E $\leq$ 38,000 eV, proton densities with the LEPEDEA instrumentation on IMP-6. With these measurements we are able to determine the density and temperature of the thermal protons and the relative contributions of the thermal and suprathermal components to the total proton densities in the region between the plasmapause and magnetopause.

II. INSTRUMENTATION

The plasma wave and charged particle measurements reported here were obtained with instrumentation on the satellite IMP-6 (Explorer 43). IMP-6 was launched on March 13, 1971, into an orbit with initial perigee and apogee geocentric radial distances of 6620 km and 211,250 km, respectively, and an inclination of 28.6°. The plasma wave antennas on IMP-6 comprise two long dipole antennas with tip-to-tip lengths of 53.5 and 92.5 meters for electric field measurements and three mutually orthogonal loop antennas for magnetic field measurements. Two 16-channel spectrum analyzers, one connected to an electric antenna and the other connected to a magnetic antenna, are used to make spectrum measurements over the frequency range from 20 Hz to 200 Hz. Two wideband receivers are also included to provide broadband coverage of the frequency ranges from 10 Hz to 1 kHz and from 650 Hz to 30 kHz, depending on the particular mode of operation selected. Further details of the plasma wave instrumentation on IMP-6 are given by Gurnett and Shaw [1973].

The Low Energy Proton and Electron Differential Energy Analyzer, or LEPEDEA, on IMP-6 provides measurements of the differential energy spectra and angular distributions of proton and electron intensities over the energy range 10 eV $\leq$ E $\leq$ 40,000 eV. These electrostatic analyzers are capable of simultaneous determinations

of proton and electron intensities within each of 16 energy band-passes. The axes of the fields-of-view of the LEPEDEA are directed normal to the satellite spin axis. The spin axis of IMP-6 is oriented perpendicular to the ecliptic plane to within a few degrees.

III. OBSERVATIONS

With the IMP-6 plasma wave measurements, Gurnett and Shaw [1973] have identified a noise band consisting of electromagnetic waves trapped in the magnetosphere at frequencies above the local electron plasma frequency. This noise band frequently has a very sharply defined lower cutoff at the local electron plasma frequency. The cutoff in the noise spectrum is caused by the reflection of ordinary mode waves at the local electron plasma frequency. An example of this noise band is illustrated in Figure 1 which shows the spectrum analyzer data for an outbound IMP-6 pass on April 6, 1972, in the local-morning sector of the magnetosphere. The ordinate for each frequency channel is proportional to the logarithm of the electric field strength in the channel. The interval from the baseline of one channel to the baseline of the next higher channel represents a dynamic range of 100 db. The vertical bars denote the average field strength over an interval of 81.8 seconds and the dots represent the maximum field strength over the same interval. Trapped electromagnetic noise of the type discussed by Gurnett and Shaw is clearly evident in the 5.62 and 10.0 kHz channels in Figure 1, extending throughout the region from the plasmapause to the magnetopause. The plasmapause location at about 1710 UT can be identified from the rapid decrease in the frequency of the upper hybrid resonance

noise band, as indicated in Figure 1, and by the abrupt increase in the electric field interference generated by the spacecraft solar array in the four lowest frequencies of the spectrum analyzer [see discussion by Gurnett and Shaw, 1973]. The magnetopause position at 0020 UT is indicated by an abrupt decrease in the intensities of the trapped electromagnetic noise. Further direct support for this identification of the magnetopause position is given later with the plasma measurements. The sharp lower cutoff frequency of the trapped electromagnetic noise is shown in the frequency-time spectrogram of Figure 2. The lower cutoff frequency is first clearly evident at about 8.5 kHz at 1820 UT and subsequently decreases to a minimum value of about 4.0 kHz at 2005 UT. As shown by Gurnett and Shaw [1973], this cutoff is at the local electron plasma frequency. Small fluctuations in the cutoff frequency, presumably due to electron density irregularities, are present on a time scale of a few minutes.

Since the cutoff frequency is sharply defined the plasma frequency can be determined with excellent accuracy, typically to within $\pm$ 1 percent. The electron density, n_e, can then be computed from the plasma frequency, f_p, using the equation (cgs units)

$$n_e = \frac{\pi m_e}{e^2} f_p^2 , \qquad (1)$$

where e is the electron charge and m_e is the electron mass. It should be noted that the electron density given by equation (1) is

the total electron density, independent of the electron energy, provided the electrons are not relativistic. For all magnetospheric regions of interest here relativistic electrons constitute a negligible fraction, $< 1\%$, of the total electron density.

The electron and proton intensities measured with the LEPEDEA during this outbound pass are shown in the energy-time spectrograms of Plate 1. The ordinate of each spectrogram is electron energy in units of electron volts, and the abscissa is universal time. The detector responses are color-coded from blue to red (low to high detector responses) according to the log scale shown on the right side of the spectrogram. The four uppermost spectrograms give the proton energy spectra in each of four quadrants. From top to bottom the angular fields of view of the detector are directed toward the sun, toward local dawn, away from the sun, and toward local dusk, respectively, as indicated by the sketch of the viewing quadrant to the left of each spectrogram. A sector of width 40° and centered in the solar direction has been eliminated from the quadrant directed toward the sun. This subsector spans th solar-wind ion flow and is processed separately. The fifth panel from the top in Plate 1, labeled GM tube, displays the responses of a thin-windowed Geiger-Mueller tube which is sensitive to electrons with energies $E \geq 45$ keV and protons with energies $E \geq 650$ keV. The responses of this detector are also sectored into four quadrants and are color-coded according to the color of the viewing quadrant

sketches shown in the top four spectrograms. The bottom spectrogram in Plate 1 gives the electron energy spectrum averaged over a complete rotational period of the spacecraft.

The position of the magnetopause at about 0020 UT is clearly evident in the observations shown in Plate 1 in the abrupt decrease of the GM tube counting rates and the decreases of the average electron and proton energies as the spacecraft passes through the magnetopause. The bow shock is located at about 0315 UT as indicated by a rapid decrease in the magnetosheath proton intensities and the appearance of solar wind proton fluxes at ~ 1-keV in the sunward-viewing quadrant. Proton energy spectra for this pass are shown in Figure 3 at three selected locations between the plasmapause (at 1710 UT) and the magnetopause (at 0020 UT). Two distinct components are evident in these energy spectra. There is a broad energetic component extending from several hundred eV to greater than ten keV, with a maximum at several keV. This energetic component corresponds to that of the quiescent proton ring current [Frank, 1967a] and is encountered throughout the region between the plasmapause and magnetopause. Near the plasmapause the spectrum of the ring current protons broadens markedly toward lower energies. At low energies, less than 100 eV, a second component, rapidly increasing in intensity toward lower energies, can be seen in the spectra observed at 1822 UT and 2010 UT. This low-energy component is also discernible in the proton spectrograms of Plate 1 at about 1720 UT through 1900 UT. As shown by the series of spectra in Figure 3 and

by the proton spectrograms of Plate 1 the intensities of this low-energy component decrease rapidly with increasing radial distance and are completely undetectable after about 2120 UT.

To determine the contribution of the hot suprathermal ring-current protons to the total proton density we have computed the densities of protons with energies 88 eV $\leq$ E $\leq$ 38,000 eV by using the direct observations of differential energy spectra of proton intensities with the LEPEDEA. The lower integration limit of 88 eV used in these computations is chosen to avoid any contribution from the aforementioned low-energy component of the proton spectrum. The upper integration limit of 38,000 eV is the upper limit of the LEPEDEA energy range. Although the energies of the ring current protons do extend above 38,000 eV these protons make only a relatively minor contribution to the proton densities because of the rapidly decreasing intensities with increasing energy. The proton (88 eV $\leq$ E $\leq$ 38,000 eV) densities have been computed from the spin-averaged directional intensities of protons in order to reduce errors caused by anisotropies in the angular distributions. For this pass the angle between the spin axis and the predicted geomagnetic field direction varied from about 67° to 75°. The intensity anisotropy can, therefore, be determined over a large range of pitch angles. Throughout the region of interest, the observed anisotropies over this range of pitch angles were less than 25 percent. It is conservatively estimated that the error in determining the proton density, which is attributable to this anisotropy, is less than $\pm$ 5%. When all sources

of error due to intensity anisotropies and detector calibrations are considered, it is judged that the determination of proton densities with the LEPEDEA is accurate to within ± 10 percent.

The results of the combined plasma wave and LEPEDEA density measurements are shown in Figure 4. The solid curve shows the total electron density as determined from the plasma frequency cutoff of the electromagnetic noise band shown in Figure 2. The dashed curve shows the 88 eV ≤ E ≤ 38,000 eV proton density as measured with the LEPEDEA. Since the total electron density and the total proton density must be equal to maintain charge neutrality, the difference between the two number densities in Figure 4 must be attributed to protons with energies not in the range 88 eV ≤ E ≤ 38,000 eV. Because of the rapidly decreasing proton intensities with high energies, this difference cannot be due to protons with energies E ≥ 38,000 eV. The observed difference between the two densities in Figure 4 must, therefore, be due to "thermal" protons with energies E ≤ 88 eV. The high-energy tail of these "thermal" protons apparently is associated with the low-energy component of the proton spectra shown in Figure 3.

It is evident in Figure 4 that, from 1820 UT to about 2120 UT, the low-energy thermal component accounts for a significant fraction, 20 to 50 percent, of the total proton density. At about 2120 UT, the density of the 88 eV ≤ E ≤ 38,000 eV "suprathermal" protons increases abruptly. At this same time the low-energy, E ≤ 88 eV, component of the proton spectrum disappears below the thresholds of

the LEPEDEA measurements (see Figure 3) and the thermal proton density, given by the difference between the two curves in Figure 4, goes to essentially zero. In this region beyond 2120 UT, out to the limit of our observations at 2250 UT, the proton distribution appears to consist almost entirely of suprathermal ring current protons with essentially no detectable low-energy thermal component. The close agreement between the two density measurements for this and several other similar passes can also be taken as a reassuring confirmation of the overall accuracy ($\pm$ 10%) of the LEPEDEA density determination.

IV. DISCUSSION

These simultaneous measurements of the total electron densities and the proton (88 eV $\leq$ E $\leq$ 38,000 eV) densities provide direct measurements of the thermal proton densities in the low density region between the plasmapause and magnetopause. The high-energy tail of the thermal proton distribution can be detected also in the lowest energy channel of the LEPEDEA. Since independent measurements can be made of the thermal proton density and the directional intensity of the high-energy tail of the thermal distribution, it is possible to make a quantitative determination of the temperature of the thermal protons, assuming that these protons have a Maxwellian velocity distribution. An example for which we have determined the thermal proton temperature using this technique is summarized in Figure 5 which shows the proton velocity distribution function $f_p(v)$ computed at two times during the pass analyzed in the previous section. These times, 2100 UT and 2130 UT, are just before and just after the abrupt decrease in the thermal plasma density at 2120 UT (see Figure 4). The distribution function has been computed from the spin-averaged directional intensities and with the assumption that the angular distribution is isotropic. This assumption is supported by the near isotropy of the observed angular distribution at these times. Directional intensity measurements

were not obtained at pitch angles near or within the loss cone where the actual distribution function is almost certainly not isotropic; however, these protons only represent a minor portion of the total proton population. At 2100 UT the thermal proton density is 0.2 protons cm^{-3}. Using this density the temperature of the Maxwellian velocity distribution has been adjusted so that the high-energy tail intercepts the value for the low-energy component of the proton distribution function determined with the LEPEDEA. The best fit in this case was obtained with a temperature of T_p = 80,000°K. Investigation of other passes through the region between the plasmapause and magnetopause indicates that this temperature is not unusual.

Since the ionosphere is thought to be the source of the low-energy thermal plasma observed at high altitudes in the magnetosphere [Banks, 1972], it is interesting to note that the thermal proton temperatures obtained with these IMP-6 observations are much higher than typical ionospheric temperatures of about 1000°K to 2000°K. However our thermal proton temperatures are in close agreement with the results of Serbu and Maier [1970] who reported ion temperatures of typically 100,000°K in the region beyond the plasmapause using measurements from the OGO-5 spacecraft. Although our results confirm the ion temperatures obtained by Serbu and Maier [1970] our proton densities, which are usually about 1 cm^{-3} or less in the region between the plasmapause and magnetopause, are a factor of 10 to 100 smaller than those reported by Serbu and Maier, but are in

agreement with densities reported by Taylor et al., [1970] and Chappell et al., [1971].

Abrupt decreases in the thermal proton densities to values much less than the suprathermal proton densities, such as that at about 2120 UT in Figure 4, are another feature frequently observed beyond the plasmapause with the IMP-6 instruments. For the example shown in Figure 4 this decrease is accompanied by a marked increase in the small scale, few minutes, irregularities in the electron densities and by an abrupt onset of electrostatic electron cyclotron emissions of the type discussed by Kennel et al., [1970] near half-integral multiples of the electron cyclotron frequency. These electrostatic electron cyclotron emissions can be seen at about 1 kHz in Figure 2 commencing at approximately 2127 UT. Similar observations during other spacecraft traversals of these regions suggest that these electrostatic electron cyclotron emissions are quenched whenever the density of low-energy thermal plasma exceeds a certain small fraction, on the order of 5 percent, of the suprathermal plasma density.

ACKNOWLEDGMENTS

This research was supported in part by the National Aeronautics and Space Administration under Contracts NAS5-11074 and NAS5-11039 and Grant NGL-16-001-043 and by the Office of Naval Research under Grant N00014-68-A-0196-0009.

REFERENCES

Banks, P. M., Behavior of thermal plasma in the magnetosphere and topside ionosphere, Critical Problems of Magnetospheric Physics, Proceedings of the Joint COSPAR/IAGA/URSI Symposium, Madrid, Spain, 1972.

Brice, N., and C. Lucas, Influence of magnetospheric convection and polar wind on loss of electrons from the outer radiation belt, J. Geophys. Res., 76, 900, 1971.

Chappell, C. R., K. K. Harris, and G. W. Sharp, The dayside of the plasmasphere, J. Geophys. Res., 76, 7632, 1971.

Cornwall, J. M., F. V. Coroniti, and R. M. Thorne, Turbulent loss of ring current protons, J. Geophys. Res., 75, 4699, 1970.

DeForest, S. E., and C. E. McIlwain, Plasma clouds in the magnetosphere, J. Geophys. Res., 76, 3587, 1971.

Frank, L. A., On the extraterrestrial ring current during geomagnetic storms, J. Geophys. Res., 72, 3753, 1967a.

Frank, L. A., Initial observations of low-energy electrons in the earth's magnetosphere with OGO 3, J. Geophys. Res., 72, 185, 1967b.

Gurnett, D. A., and R. R. Shaw, Electromagnetic radiation trapped in the magnetosphere above the plasma frequency, accepted for publication, J. Geophys. Res., 1973.

Kennel, C. F., and H. E. Petschek, Limit on stably trapped particle fluxes, J. Geophys. Res., 71, 1, 1966.

Kennel, C. F., F. L. Scarf, R. W. Fredricks, J. H. McGehee, and F. V. Coroniti, VLF electric field observations in the magnetosphere, J. Geophys. Res., 75, 6136, 1970.

Russell, C. T., and R. M. Thorne, On the structure of the inner magnetosphere, Cosmic Electrodynamics, 1, 67, 1970.

Serbu, G. P., and E. J. R. Maier, Observations from OGO 5 of the thermal ion density and temperature within the magnetosphere, J. Geophys. Res., 75, 6102, 1970.

Taylor, H. A., H. C. Brinton, and M. W. Pharo, III, Contraction of the plasmasphere during geomagnetically disturbed periods, J. Geophys. Res., 73, 961, 1968.

Taylor, H. A., H. C. Brinton, and A. R. Deshmukh, Observations of irregular structure in thermal ion distributions in the dusk-side magnetosphere, J. Geophys. Res., 75, 2481, 1970.

Thorne, R. M., E. J. Smith, R. K. Burton, and R. E. Holtzer, Plasmaspheric hiss, J. Geophys. Res., 78, 1581, 1973.

Vasyliunas, V. M., A survey of low-energy electrons in the evening sector of the magnetosphere with OGO 1 and OGO 3, J. Geophys. Res., 73, 2839, 1968.

FIGURE CAPTIONS

Plate 1 Energy-time spectrograms of the electron and proton intensities observed during the pass shown in Figure 1. The top four spectrograms are the proton intensities in four directional quadrants: from top to bottom, looking toward the sun, toward local dawn, away from the sun, and toward local dusk. The fifth panel from the top displays the GM tube responses and the bottom spectrogram gives the spin-averaged electron intensities.

NOTE: Plate 1 is to be published in color.

Figure 1 An outbound IMP-6 pass at local morning on April 6, 1972, with trapped electromagnetic noise above the plasma frequency ($f > f_p$) in the region between the plasmapause and the magnetopause. Note the abrupt termination of the $f > f_p$ noise band at the magnetopause.

Figure 2 Electric field frequency-time spectrogram illustrating the sharp lower cutoff frequency of the trapped $f > f_p$ noise band shown in Figure 1. The cutoff frequency is at the local electron plasma frequency. The small scale

variations in the cutoff frequency are due to irregularities in the electron densities.

Figure 3 The spin-averaged directional proton energy spectra measured with the LEPEDEA at three selected points during the pass shown in Figures 1 and 2 and Plate 1. The suprathermal protons with energies $E \geq 88$ eV and peak intensities at several keV constitute the quiescent ring current. The low-energy $E \leq 88$ eV component evident in the 1822 UT and 2010 UT spectra is the high-energy tail of the thermal proton distribution.

Figure 4 Comparison of the total electron densities obtained from the plasma frequency cutoff and the suprathermal, $88 \text{ eV} \leq E \leq 38{,}000$ eV. proton densities obtained with the LEPEDEA. Note that after about 2120 UT essentially the entire proton population consists of suprathermal protons.

Figure 5 The proton velocity distribution functions for just before and just after the abrupt decrease in the thermal proton density at 2120 UT. The thermal proton temperature has been determined by fitting the high-energy tail of the Maxwellian thermal distribution to the low-energy component of the proton distribution determined with the LEPEDEA.

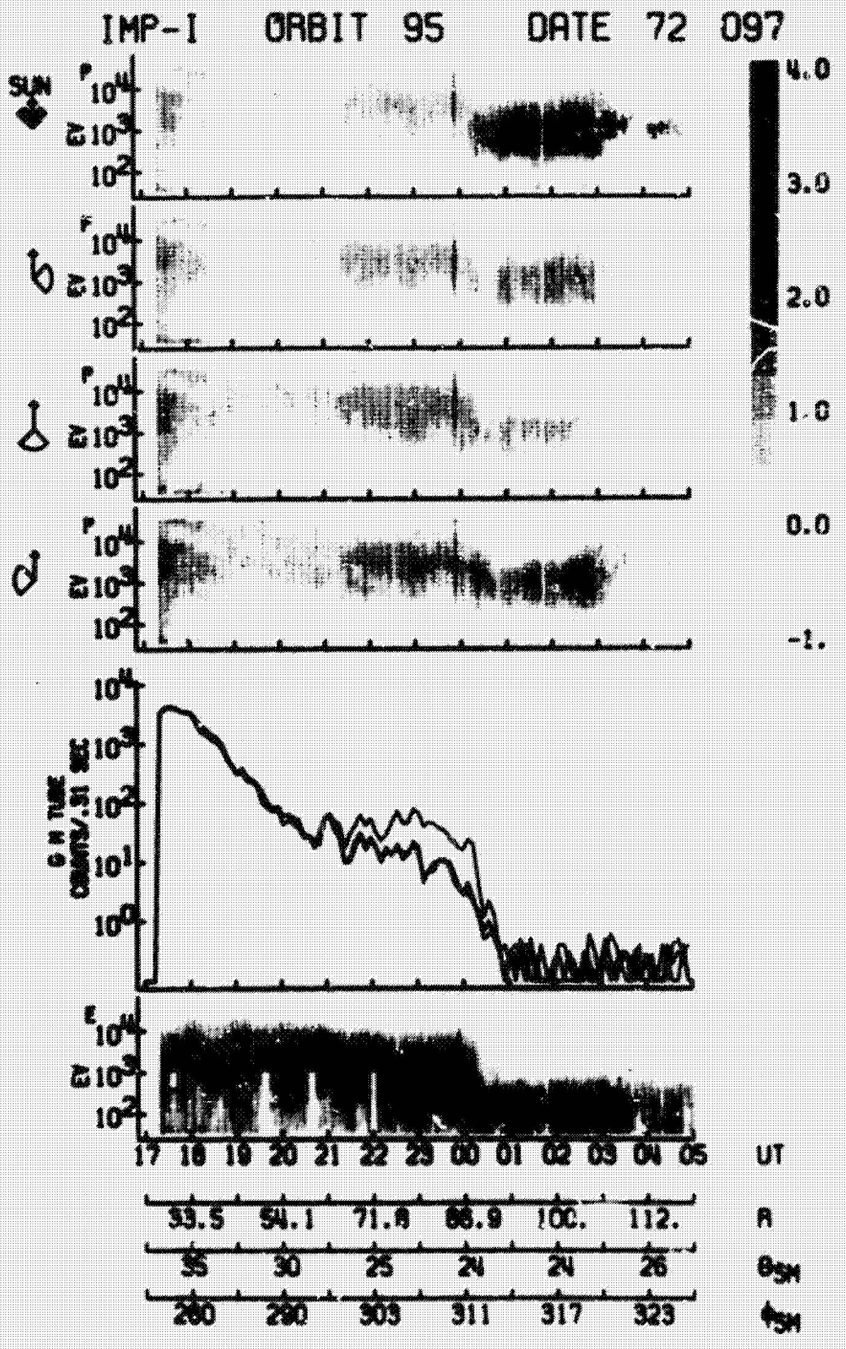
IMP-I ORBIT 95 DATE 72 097
SUN
P
E
10^4
10^3
10^2
4.0
3.0
2.0
1.0
0.0
-1.
10^4
10^3
10^2
10^1
10^0
17 18 19 20 21 22 23 00 01 02 03 04 05
UT
33.5 54.1 71.8 88.9 100. 112.
R
35 30 25 24 24 26
θ_{SM}
280 280 303 311 317 323
ϕ_{SM}

Plate 1

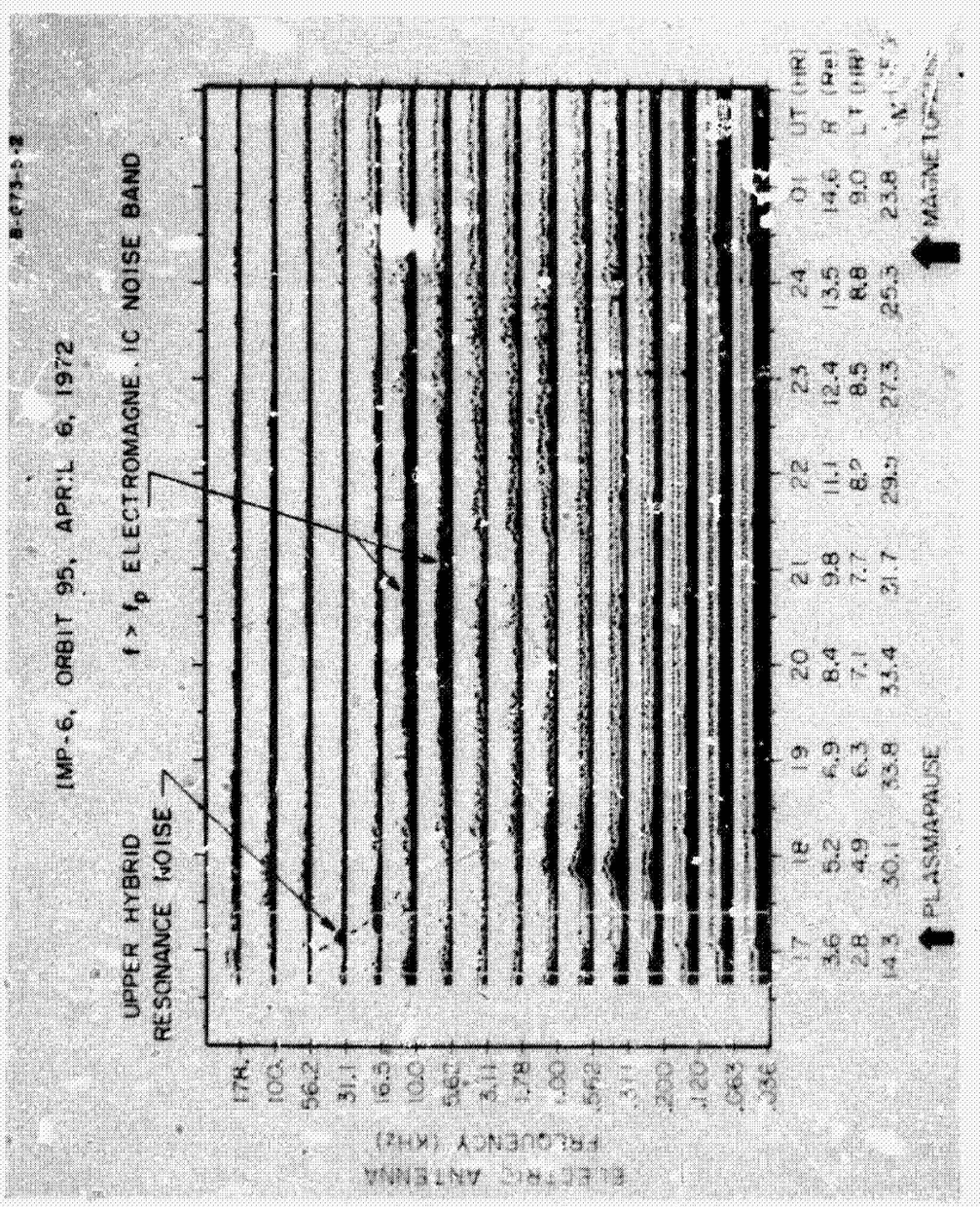
IMP-6, ORBIT 95, APRIL 6, 1972
UPPER HYBRID RESONANCE NOISE
f > fp ELECTROMAGNETIC NOISE BAND
ELECTRIC ANTENNA FREQUENCY (KHZ)
17R
105
56.2
31.1
16.3
100
56.2
31.1
17.8
10.0
5.62
3.11
2.00
1.20
.562
.316
17 18 19 20 21 22 23 24 01 UT (HR)
3.6 5.2 6.9 8.4 9.8 11.1 12.4 13.5 14.6 R (Re)
2.8 4.9 6.3 7.1 7.7 8.2 8.5 8.8 9.0 LT (HR)
14.3 30.1 33.8 33.4 31.7 29.5 27.3 25.3 23.8
PLASMAPAUSE
MAGNETOPAUSE

Figure 1

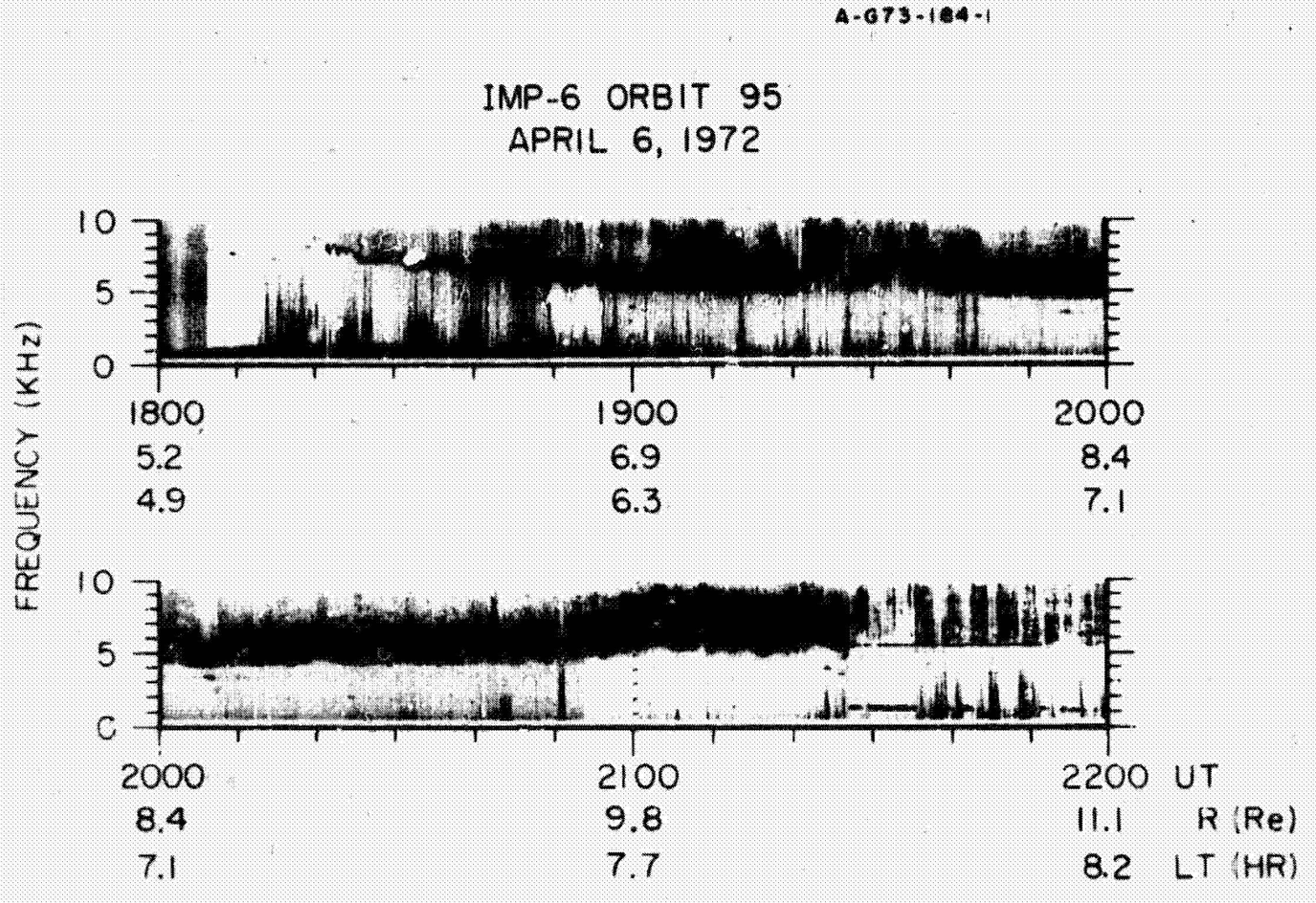
A-G73-184-1
IMP-6 ORBIT 95
APRIL 6, 1972
FREQUENCY (KHz)
10
5
0
1800
1900
2000
5.2
6.9
8.4
4.9
6.3
7.1
10
5
0
2000
2100
2200 UT
8.4
9.8
11.1 R (Re)
7.1
7.7
8.2 LT (HR)

Figure 2

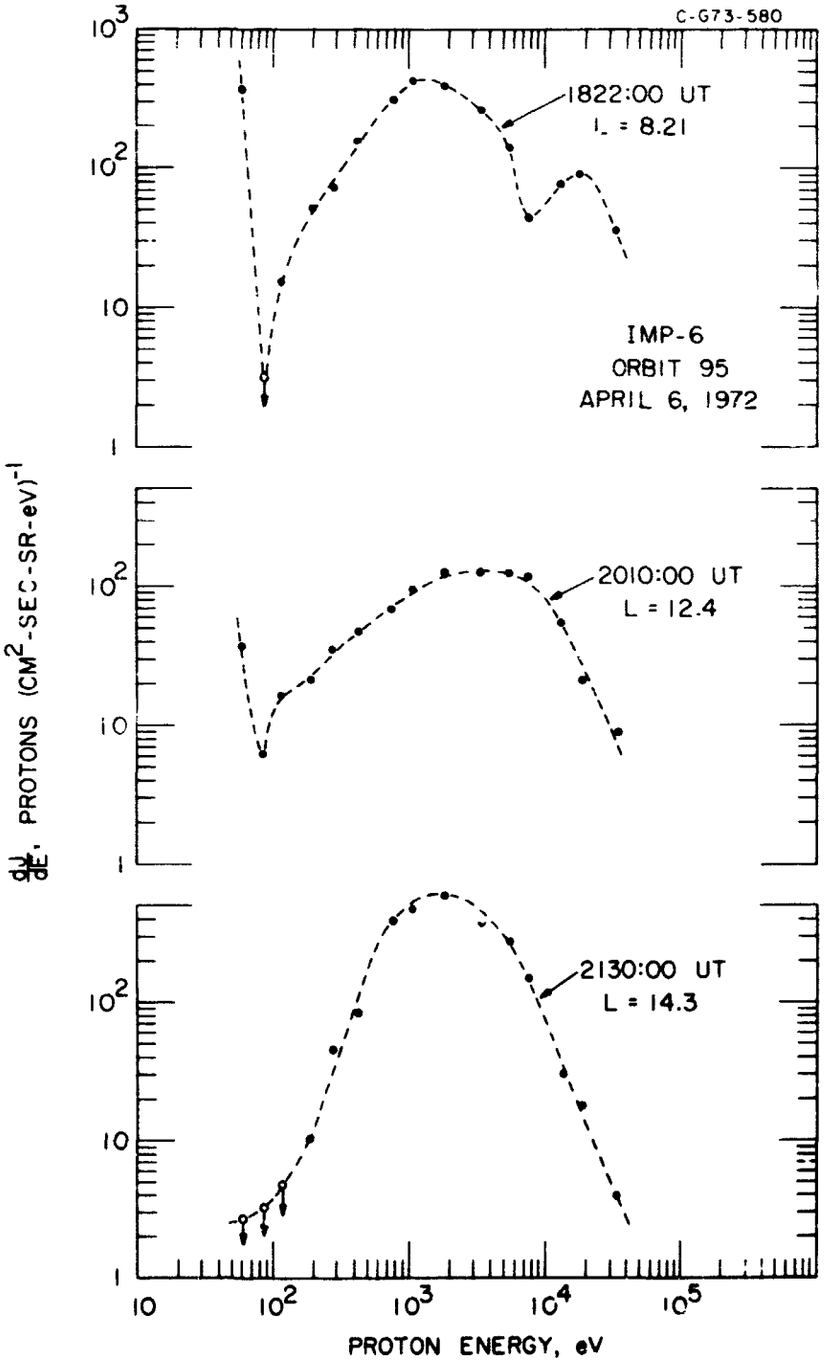
C-G73-580
1822:00 UT
L = 8.21
IMP-6
ORBIT 95
APRIL 6, 1972
2010:00 UT
L = 12.4
2130:00 UT
L = 14.3
dJ/dE, PROTONS (CM²-SEC-SR-eV)⁻¹
PROTON ENERGY, eV

Figure 3

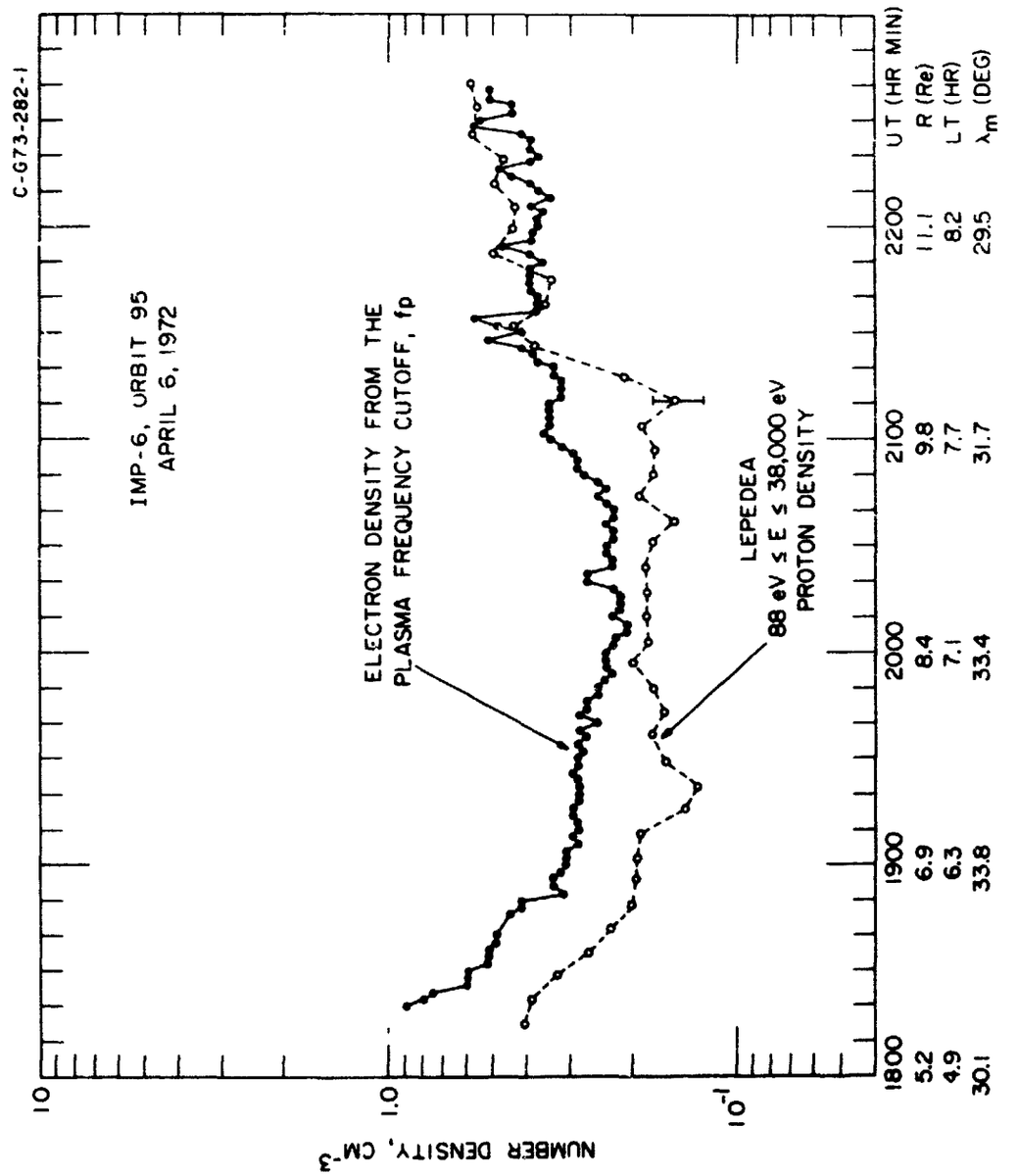
C-G73-282-1
IMP-6, ORBIT 95
APRIL 6, 1972
ELECTRON DENSITY FROM THE
PLASMA FREQUENCY CUTOFF, fp
LEPEDEA
88 eV ≤ E ≤ 38,000 eV
PROTON DENSITY
NUMBER DENSITY, CM⁻³
10
1.0
10⁻¹
1800
2000
2100
2200
UT (HR MIN)
5.2
8.4
9.8
11.1
R (Re)
4.9
7.1
7.7
8.2
LT (HR)
30.1
33.4
31.7
29.5
λm (DEG)

Figure 4

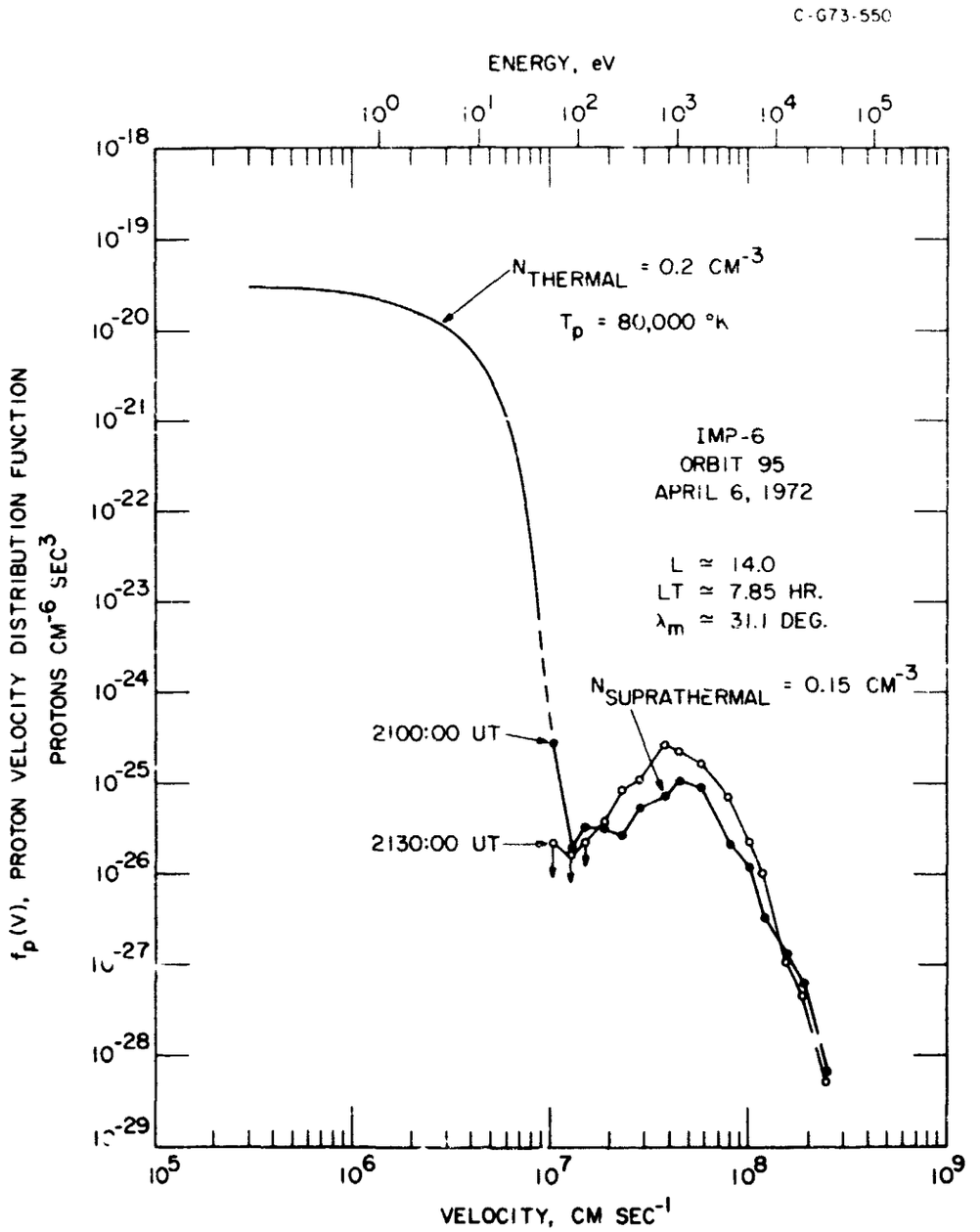
C-G73-550
ENERGY, eV
10^0
10^1
10^2
10^3
10^4
10^5
10^{-18}
10^{-19}
10^{-20}
10^{-21}
10^{-22}
10^{-23}
10^{-24}
10^{-25}
10^{-26}
10^{-27}
10^{-28}
10^{-29}
$N_{THERMAL}$ = 0.2 CM^{-3}
T_p = 80,000 °K
IMP-6
ORBIT 95
APRIL 6, 1972
L ≃ 14.0
LT ≃ 7.85 HR.
λ_m ≃ 31.1 DEG.
$N_{SUPRATHERMAL}$ = 0.15 CM^{-3}
2100:00 UT
2130:00 UT
$f_p(V)$, PROTON VELOCITY DISTRIBUTION FUNCTION
PROTONS CM^{-6} SEC^3
10^5
10^6
10^7
10^8
10^9
VELOCITY, CM SEC^{-1}

Figure 5